DFT Analysis of $Fe(H_2O)_6^{3+}$ and $Fe(H_2O)_6^{2+}$ Structure and Vibrations; Implications for Isotope Fractionation

A. A. Jarzęcki,[†] A. D. Anbar,[‡] and T. G. Spiro*[,†]

Department of Chemistry and Center for Environmental Bioinorganic Chemistry, Princeton University, Princeton, New Jersey 08544, and Department of Earth and Environmental Sciences and Department of Chemistry, University of Rochester, Rochester, New York 14627

Received: August 13, 2003; In Final Form: February 3, 2004

Density functional theory (DFT) calculations of structure and vibrational modes are reported for the ferrous and ferric hexaaquo ions, using B3LYP gradient-corrected hybrid density functionals, standard 6-31G* basis sets on the O and H atoms, and Ahlrichs' valence triple-ζ (VTZ) basis set on the Fe atom. The effect of hydrogen bonding in solvents or in crystals has been approximated with the polarizable continuum model (PCM). The optimized structures predict a regular FeO_6 octahedron for $Fe(H_2O)_6^{3+}$, as expected, but inequivalent Fe−O distances (C_i symmetry) for $Fe(H_2O)_6^{2+}$, reflecting Jahn−Teller distortion. PCM shortens the Fe−O distances and produces excellent agreement with crystallographic data. In vacuo, DFT produces a stable T_h structure for $Fe(H_2O)_6^{3+}$, with the H_2O molecules lying in FeO_4 planes, but PCM induces tilting and rotation of the H_2O molecules. This effect is shown to be an artifact of the PCM methodology, but it does not significantly affect the computed Fe−O stretching and bending frequencies, which are the main determinants of the equilibrium isotope fractionation. The DFT-computed vibrational modes are consistent with reported Raman and infrared spectra of the complexes in crystals, except that assigned O−Fe−O bending frequencies are higher than predicted, probably owing to strong hydrogen bonding in the ionic lattices. The computation produces a significant revision of the $^{54/56}$Fe isotope sensitivity of the $Fe(H_2O)_6^{3+}$ and $Fe(H_2O)_6^{2+}$ vibrational partition functions, relative to a previous estimate from an empirical FeO_6 force field. The difference arises in part from lowered bending mode frequencies and in part from including modes of the bound H_2O (rocking, wagging, and twisting), which have nonnegligible $^{54/56}$Fe isotope shifts. Excellent agreement is found with the recently determined isotope fractionation factor for the $Fe(H_2O)_6^{3+/2+}$ exchange equilibrium. DFT vibrational analysis of metal complexes can contribute significantly to the evaluation of geochemical and biogeochemical isotope fractionation data.

Introduction

The isotopic abundances of many elements in the environment and in biology vary by as much as ∼1% because of the effects of isotope mass on chemical reaction rates and equilibrium constants. Studies of such variations are of particular utility in the geosciences.[1] Recent analytical advances have made it possible to study isotopic abundance variations of transition metals, leading to reports of natural and experimental isotope variations of 0.01−1% for Cu, Zn, Fe, Cr, Mo, Cd, and even Tl.[2−13] Fe isotope research has drawn particular attention because of the ubiquity of this element in the environment and its importance in biology. As a result, Fe isotope analyses may prove useful in a range of applications ranging from geology to biology to cosmochemistry (e.g., refs 14−16).

Theoretical study of transition metal isotope effects lags considerably behind analytical (mass spectrometric) capabilities. The theory of equilibrium isotope fractionation—differences in isotope abundances between compounds at equilibrium—is well established.[17−20] Such fractionation results from the mass dependence of bond strengths in the equilibrating compounds. These differences can be readily related to isotope sensitivity of vibrational frequencies and hence vibrational partition functions. Therefore, equilibrium isotope effects between two or more molecules can be predicted from vibrational spectra of the isotopically substituted molecules (isotopomers). However, such data are often unavailable or incomplete, and mode assignments may be questionable. Consequently, accurate force field models are needed to predict the magnitude of such effects.

In this study, we compute structures and vibrational modes for $Fe(H_2O)_6^{3+}$ and $Fe(H_2O)_6^{2+}$. These ions are of longstanding chemical interest, and high-quality data are available for comparison, from crystallography[21,22] and vibrational spectroscopy.[23−25] Our investigation is motivated by recent mass spectrometric determinations of the magnitude of the equilibrium isotope effect between these complexes.[7,26] Experimental determinations differ by about a factor of 2 from theoretical expectations that utilize published vibrational assignments and a modified Urey−Bradley force field (MUBFF).[27] Here, we use density functional theory (DFT) to reexamine vibrational assignments for these complexes and predict the effects of isotope substitution on vibrational frequencies. The broader implications for geoscience applications of Fe isotope research are discussed in a companion paper.[28]

Computational Details

Computations were performed with the Gaussian 98 program package,[29] using the B3LYP gradient-corrected hybrid density

* Corresponding author.
[†] Princeton University.
[‡] University of Rochester.

10.1021/jp036418b CCC: $27.50
Published on Web 03/17/2004

TABLE 1: Calculated and Experimental Bond Distances (Å) and Angles (deg) in $Fe(H_2O)_6^{3+}$

	B3LYP[a]	PCM B3LYP[b]		$CsFe(SO_4)_2 \cdot 12H_2O$[c]	$CsFe(SeO_4)_2 \cdot 12H_2O$[c]
	T_h	T_h[d]	S_6[e]	S_6	S_6
Fe−O	2.039	1.996	2.005	1.994(1)	2.002(1)
O−Fe−O	90.00	90.00	90.01	90.9(1)	90.5(1)
O−H	0.982	0.995	0.998	0.995(3)	1.002(2)
H−O−H	106.76	108.28	107.31	110.4(2)	108.0(2)
Fe−OH_2 tilt	0.00	0.00	24.83	0.6(10)	18.6(10)
Fe−OH_2 rot	0.00	0.00	4.77	–	–

[a] B3LYP/6-31G* and Ahlrichs' VTZ level of theory (in vacuo). [b] PCM B3LYP/6-31G* and Ahlrichs' VTZ level of theory in polarizable continuum model ($\epsilon = 78.4$). [c] Low-temperature neutron diffraction data.[21] Dashes indicate not reported experimental data. [d] Constrained to T_h symmetry. [e] Fully optimized PCM structure.

TABLE 2: Calculated and Experimental Bond Distances (Å) and Angles (deg) in $Fe(H_2O)_6^{2+}$

	B3LYP	PCM B3LYP	$(NH_4)_2[Fe(H_2O)_6](SO_4)_2$[a]
$Fe-O_1$	2.140	2.125	2.143(2)
$Fe-O_2$	2.136	2.106	2.136(2)
$Fe-O_3$	2.110	2.086	2.098(2)
O_1–Fe−O_2	89.99	89.66	89.25(6)
O_1–Fe−O_3	91.19	91.33	91.02(6)
O_2–Fe−O_3	90.01	90.10	90.86(6)
H−O_1	0.973	0.982	0.83(3)
H−O_2	0.973	0.983	0.82(3)
H−O_3	0.973	0.980	0.95(3)
H−O_1–H	106.45	105.07	–
H−O_2–H	106.74	105.72	–
H−O_3–H	106.85	106.50	–
Fe−O_1H_2 tilt	0.06	34.48	–
Fe−O_1H_2 rot	9.38	28.19	–
Fe−O_2H_2 tilt	0.62	39.62	–
Fe−O_2H_2 rot	4.82	10.59	–
Fe−O_3H_2 tilt	4.02	9.13	–
Fe−O_3H_2 rot	0.14	7.30	–

[a] Ammonium Tutton salt, X-ray data.[22] Dashes indicate not reported experimental data.

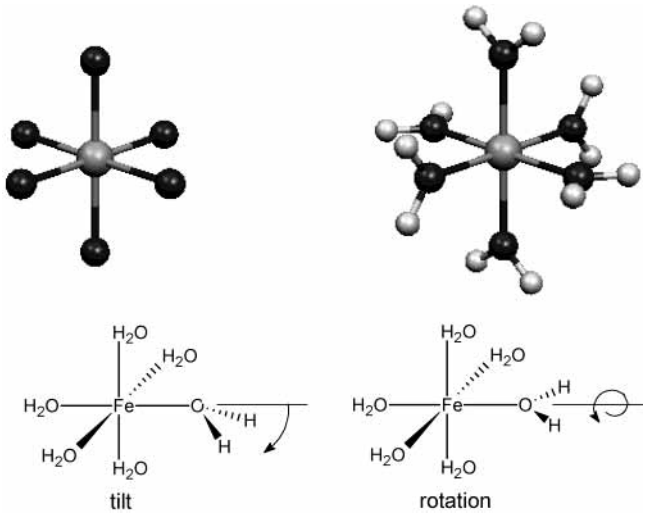

Figure 1. Illustration of (top) the central FeO_6 octahedron and of the water orientations in the T_h structure and (bottom) the H_2O tilting and rotation coordinates.

functional to optimize structures and calculate vibrational frequencies. This functional combines Becke's three-parameter hybrid of the gradient-corrected exchange (B3)[30] and the exact Hartree−Fock (HF) exchange with the Lee, Yang, and Parr (LYP)[31] gradient-corrected correlation functional.

For the basis set functions, we applied the 5-d component set, comprised of the standard 6-31G* basis functions[32−36] on the O and H atoms and Ahlrichs' valence triple-ζ (VTZ) basis set on the Fe atom.[37] Previous applications of the B3LYP functional in combination with these basis sets proved to produce quite reliable structures and frequencies for various transition metal complexes[38,39] and metalloporphyrins.[40,41]

Since the aquo ions are well-known to be high-spin, only the sextet state for Fe^{3+} and the quintet state for Fe^{2+} were evaluated. The complexes were treated in vacuo and then imbedded in the polarizable continuum model (PCM)[42] to account for the presence of solvent. In the PCM approach the solute is placed in a polarizable cavity formed by the envelope of spheres centered on the atoms or the atomic groups. Inside the cavity the dielectric constant is the same as in vacuo, while outside it takes the value of the desired solvent [$\epsilon = 78.4$ for water]. The PCM is one of the most used and reliable continuum solvation procedures.[42−46]

Results and Discussion

Structures. Computed structural parameters are given in Tables 1 and 2, and compared with crystallographic data. For $Fe(H_2O)_6^{3+}$ low-temperate neutron data are available for the cesium sulfate and selenate alums,[21] $CsFe(SO_4)_2 \cdot 12H_2O$ and $CsFe(SeO_4)_2 \cdot 12H_2O$, while for $Fe(H_2O)_6^{2+}$ we chose X-ray data for the ammonium Tutton salt,[22] $(NH_4)_2[Fe(H_2O)_6](SO_4)_2$.The $Fe(H_2O)_6^{3+}$ complex was optimized as an FeO_6 octahedron, with the water H atoms arranged in T_h symmetry (Figure 1). This procedure converged to a structure (second column of Table 1) with all positive vibrational frequencies in vacuo, but in the PCM model three frequencies were negative. Removal of the T_h symmetry constraint led to an S_6 PCM structure, in which the water molecules are tilted and rotated with respect to the FeO_4 planes (Figure 1). The energy was lowered by 1.7 kcal/mol. Structure parameters for the T_h and S_6 PCM structures are given in columns 3 and 4 of Table 1.

To investigate the source of symmetry lowering in the PCM computation, we applied the same DFT PCM methodology to the ion $Al(H_2O)_6^{3+}$. Once again a T_h structure was stable in vacuo, but application of PCM and optimization of the geometry produced an S_6 structure with pronounced tilting of the water molecules, 25.1°. Since Al^{3+} has a closed shell electronic structure, the water tilting cannot be an intrinsic feature of the bonding orbitals. We attribute the tilting to an artifact of the PCM methodology, which applies a polarizable cavity of fixed dimension.

To test this idea we applied another model, IPCM (isodensity polarizable continuum model), in which the surface of the continuum is adjusted and optimized to the complex. This method is unable to optimize the geometry of the complex itself, but it does allow comparison of polarization energies for alternative structures.

We applied IPCM to the $Fe(H_2O)_6^{3+}$ structures listed in Table 1 and found that the PCM T_h structure was 0.4 kcal/mol more stable than the in vacuo structure, but the PCM S_6 structure was *less* stable by 8.2 kcal/mol. Thus the bond distance changes

TABLE 3: Electron Occupation of Atomic Valence Orbitals[a]

		Fe^{3+}(B3LYP)	Fe^{3+}(PCM B3LYP)	
	Fe^{3+}, O, H	T_h	T_h	S_6
Fe	5.0	5.7621	5.9214	5.9224
$3d_\pi$	3.0	3.2446	3.2645	3.2840
$3d_\sigma$	2.0	2.3363	2.3640	2.3398
4s	0.0	0.1812	0.2929	0.2986
H_2O	8.0	7.8554	7.8326	7.8317
O				
2s	2.0	1.7516	1.7526	1.7593
2p	4.0	5.2736	5.2720	5.2656
H				
1s	1.0	0.4151	0.4040	0.4034

[a] Based on natural population analysis.[73]

induced by polarization continuum (see next section) do stabilize the structure, but the S_6 distortion must be an artifact; a polarizable continuum does not intrinsically favor water tilting or rotation.

The $Fe(H_2O)_6^{2+}$ complex required symmetry lowering to C_i even in vacuo, due to the Jahn−Teller effect (see below); the extent of tilting and rotation of the water molecules was small (column 2 of Table 2), but increased substantially in the PCM model (column 3). As in the case of $Fe(H_2O)_6^{3+}$, some of this enhanced distortion is likely to be a PCM artifact.

A different approach to modeling the solvent effects is to add explicit water molecules to build a second hydration sphere and giving an $Me(H_2O)_{18}$ cluster. Calculations of aluminum(III)[47] and scandium(III)[48] water clusters indicate that frequency shifts predicted in the PCM model show the same trends as those modeled by the nanodroplet model. The nanodroplet model, however, is computationally much more demanding.

Fe−O Distances. The Fe−O distance in $Fe(H_2O)_6^{3+}$ is 2.039 Å in vacuo but decreases by 0.04 Å upon application of the PCM, bringing the distance into agreement with the alum structures. Thus PCM significantly improves the main structure parameter in the case of $Fe(H_2O)_6^{3+}$. Low angle X-ray scattering from iron(III) in perchlorate solution gives an average Fe−O distance of 2.00 Å with uncertainty 0.01 Å.[49]

The Fe−O bonds in $Fe(H_2O)_6^{3+}$ are all equal, because Fe^{3+} has a d^5 electron configuration and is spherically symmetric. However, Fe^{2+} has a d^6 configuration, and a nominally octahedral complex is subject to Jahn−Teller distortion because one of the three d_π orbitals is doubly occupied. The X-ray structure of $(NH_4)_2[Fe(H_2O)_6](SO_4)_2$[22] reveals an essentially tetragonal $Fe(H_2O)_6^{2+}$ complex, with four 2.14 Å equatorial and two 2.10 Å axial Fe−O bonds (Table 2). The bond length differences are small, since the d_π orbitals are essentially nonbonding. The differences are much larger, ∼0.25 Å, for $Cr(H_2O)_6^{2+}$ and $Cu(H_2O)_6^{2+}$, which have an extra electron in one of the two antibonding d_σ orbitals.[22] The $Fe(H_2O)_6^{2+}$ structure computed in vacuo has almost exactly the observed bond lengths (2.14 and 2.11 Å). As with $Fe(H_2O)_6^{3+}$, application of the PCM model decreases the Fe−O distances, by 0.015−0.03 Å. In this case PCM worsens the agreement with experiment (by up to 0.03 Å), suggesting that the very close match of the in vacuo distances is fortuitous.

Bound Water. The computed O−H distances for $Fe(H_2O)_6^{3+}$ are 0.982 Å in vacuo and increase to 0.995 (T_h structure) or 0.998 (S_6 structure) Å in the PCM model, in excellent agreement with the neutron structures of the alums (Table 1). The slight increase in the PCM model reflects charge transfer away from H due to polarization. Table 3 lists computed electron populations, and shows that the 1s orbital on H loses 0.011 (T_h) or 0.017 (S_6) electron upon application of PCM. These electrons are transferred to Fe; the net occupation of the O orbitals hardly changes. A similar increase is seen in the PCM-computed O−H distances of $Fe(H_2O)_6^{2+}$, from 0.973 to 0.980−0.983 Å. The cited experimental distances are 0.83−0.95 Å, but H atoms are not accurately located via X-ray diffraction.

Even though the computed water tilting in $Fe(H_2O)_6^{3+}$ is apparently an artifact of the PCM methodology, the resulting S_6 structure is strikingly similar to that observed in $CsFe(SeO_4)_2\cdot 12H_2O$ whereas the T_h constrained PCM structure is close to that observed in $CsFe(SO_4)_2\cdot 12H_2O$. $CsFe(SO_4)_2\cdot 12H_2O$ is a β alum, in which the symmetry of the lattice constrains the $FeOH_2$ atoms to be coplanar. $CsFe(SeO_4)_2\cdot 12H_2O$ is an α alum, in which $FeOH_2$ pyramidalization is permitted; the tilt angle is 18.6° in $CsFe(SeO_4)_2\cdot 12H_2O$.[21]

These structural features are common to all β alums on the one hand and α alums on the other.[50−58] The choice of lattice is mainly determined by the relative size of the monovalent cation and of the oxyanion.[59] The lattice constraints have been exploited in comparing the electronic properties of the trivalent cation hexaaquo ions with respect to the tilting[59] and rotation[52,58,60,61] angles. Even the slight increase in the Fe−O bond length between the sulfate and selenate crystals, 1.994 to 2.002 Å, is reproduced by the PCM, when the T_h structure is allowed to relax to S_6 (1.996 to 2.005 Å; Table 1). Evidently water tilting is accompanied by a small Fe−O extension. The geometry of the complex in solution is uncertain, but analysis of the EPR and electronic spectra of $Ru(H_2O)_6^{3+}$ and $V(H_2O)_6^{3+}$ [58] indicates that the water molecules are not tilted, and that their rotation angles are determined by the Jahn−Teller effect, when present.

Vibrations

Computed Modes. Computed normal mode frequencies are listed in Tables 4 and 5, while Fe−O stretching force constants are compared in Table 6. The Fe−O force constants diminish with increasing Fe−O distance, as expected. Figure 3 shows that this dependence follows Badger's rule,[62−64] the well-known empirical relation between force constant and bond distance. Computed frequencies for the PCM model are given only for the S_6 $Fe(H_2O)_6^{3+}$ structure, since the T_h structure is unstable and cannot provide equilibrium frequencies. However, the S_6 distortion is unlikely to significantly influence the Fe−O stretching and bending frequencies, which are main determinants of the isotope fractionation (see below).

Experience has shown that DFT-derived mode frequencies are reasonably close to experimental values, but deviations are encountered, reflecting neglect of anharmonicity, basis set errors, and medium effects. With sufficient data, these can be corrected by scaling the force constants empirically, and Pulay and coworkers[38,65,66] have shown that a limited set of scaling factors can successfully reproduce experimental spectra for many classes of molecules, including metal complexes. In the present case, however, the data are limited. We tried applying the scaling factors developed for metal acetylacetonates,[38] but we found that our computed frequencies were altered very little because of compensation among the factors, some of which are higher and some lower than unity. Consequently, we have not attempted to eliminate discrepancies with experiment, and simply report the unscaled frequencies.

We are interested in the skeletal modes of the complexes and omit tabulation of the high-frequency O−H stretching and H−O−H bending modes. Since the complexes have C_i or higher symmetry, the modes factor conveniently into g- and u-symmetries (Tables 4 and 5, respectively). The former are active

TABLE 4: Calculated g-symmetry Mode Frequencies of $Fe(H_2O)_6^{3+}$ and $Fe(H_2O)_6^{2+}$ Complexes ($^{56}\nu$) [cm^{-1}], Computed Using the B3LYP Density Hybrid Functional with 6-31G* Basis Set for Ligand Atoms and Ahlrichs' VTZ for Iron, with and without the Polarizable Continuum Medium (PCM)

		$Fe(H_2O)_6^{3+}$			$Fe(H_2O)_6^{2+}$		
vibrational assignment	(O_h)	expt[a]	PCM B3LYP (S_6)	B3LYP (T_h)	expt[b]	PCM B3LYP (C_i)[c]	B3LYP (C_i)[c]
ν_5: O−Fe−O def	(T_{2g})	306 332	170 (A_g) 176 (E_g) 176 (E_g)	180 (T_g) 180 (T_g) 180 (T_g)	210[d] 231[d]	108 116 148	88 107 114
ν_2: Fe−O stretch	(E_g)	475	400 (E_g) 400 (E_g)	360 (E_g) 360 (E_g)	296	272 301	196 265
ν_1: Fe−O stretch	(A_g)	523	486 (A_g)	449 (A_g)	379	392	365
H_2O twist		−	246 (A_g) 256 (E_g) 256 (E_g)	339 (T_g) 339 (T_g) 339 (T_g)	−	234 253 261	279 291 329
H_2O wagg (out-of-plane)		−	316 (A_g) 334 (E_g) 334 (E_g)	509 (T_g) 509 (T_g) 509 (T_g)	−	63 388 468	57 364 367
H_2O rock (in-plane)		721 742 746	739 (A_g) 741 (A_g) 741 (A_g)	662 (T_g) 662 (T_g) 662 (T_g)	−	480 572 657	511 531 532

[a] Raman bands based on observations in $CsFe(SO_4)_2 \cdot 12H_2O$ and $CsFe(SeO_4)_2$.[23] [b] Raman bands observed in $FeSiF_6 \cdot 6H_2O$.[24] [c] All vibrations are of A_g symmetry. [d] Peaks shifted from these values at 15 K to 187 and 198 cm^{-1} at 300 K.

TABLE 5: As Table 4, but u-Symmetry Modes, and Also $^{56}\nu/^{54}\nu$ Isotope Ratios and Computed IR Intensities [km/mol]

		$Fe(H_2O)_6^{3+}$						$Fe(H_2O)_6^{2+}$					
			PCM B3LYP (S_6)			B3LYP (T_h)			PCM B3LYP (C_i)[a]			B3LYP (C_i)[a]	
vibrational assignment	(O_h)	expt[b]	$^{56}\nu$	$1 - {}^{56}\nu/{}^{54}\nu$	IR int	$^{56}\nu$	$1 - {}^{56}\nu/{}^{54}\nu$	expt[c]	$^{56}\nu$	$1 - {}^{56}\nu/{}^{54}\nu$	IR int	$^{56}\nu$	$1 - {}^{56}\nu/{}^{54}\nu$
ν_6: O−Fe−O def	(T_{2u})	−	108 (A_u) 112 (E_u) 112 (E_u)	0.000 18 0.000 18 0.000 18	7 74 74	127 (T_u) 127 (T_u) 127 (T_u)	0.000 08 0.000 08 0.000 08	−	79 86 107	0.000 00 0.000 81 0.001 12	69 34 45	90 98 104	0.000 67 0.000 41 0.000 10
ν_4: O−Fe−O def	(T_{1u})	304[d]	164 (A_u) 188 (E_u) 188 (E_u)	0.005 09 0.005 34 0.005 34	7 28 28	185 (T_u) 185 (T_u) 185 (T_u)	0.005 44 0.005 44 0.005 44	−	124 133 170	0.002 72 0.004 36 0.004 33	138 27 169	121 135 137	0.004 70 0.004 74 0.004 57
ν_3: Fe−O stretch	(T_{1u})	505	470 (E_u) 470 (E_u) 487 (A_u)	0.005 59 0.005 59 0.006 11	77 77 304	434 (T_u) 434 (T_u) 434 (T_u)	0.005 02 0.005 02 0.005 02	389	363 386 388	0.004 61 0.004 88 0.005 97	205 77 106	340 373 387	0.004 68 0.002 67 0.002 07
H_2O twist		−	225 (E_u) 225 (E_u) 293 (A_u)	0.000 22 0.000 22 0.000 20	286 286 4	257 (E_u) 257 (E_u) 478 (A_u)	0.000 00 0.000 00 0.000 00	−	242 266 331	0.000 04 0.000 04 0.000 30	214 80 113	189 243 421	0.000 21 0.000 41 0.000 31
H_2O wagg (out-of-plane)		−	304 (E_u) 304 (E_u) 359 (A_u)	0.000 43 0.000 43 0.000 91	1121 1121 149	532 (T_u) 532 (T_u) 532 (T_u)	0.000 24 0.000 24 0.000 24	e	137 413 470	0.002 62 0.001 98 0.000 26	360 653 598	319 345 403	0.002 87 0.003 47 0.001 12
H_2O rock (in-plane)		668	769 (E_u) 769 (E_u) 774 (A_u)	0.000 27 0.000 27 0.000 30	275 275 164	672 (T_u) 672 (T_u) 672 (T_u)	0.001 23 0.001 23 0.001 23	575	518 605 681	0.001 27 0.000 45 0.000 32	332 133 201	538 563 565	0.001 17 0.001 26 0.001 13

[a] All vibrations are of A_u symmetry. [b] IR bands observed in cesium β alums.[70] [c] IR bands observed in $FeSiF_6 \cdot 6H_2O$.[25] [d] This mode is suggested to have a substantial contribution for the wagging coordinate because of its considerable IR intensity and less than expected 50/53 Cr isotope shift in the chromium alum[70] (see discussion). [e] Obscured by a very strong band of SiF_6^{2-} at 485 cm^{-1}.[25]

TABLE 6: Fe−O Stretching Diagonal Force Constants (mdyn/Å)

	B3LYP	PCM B3LYP
$Fe^{III}-O$	1.5494	1.7375
$Fe^{II}-O_1$	0.8432	1.0060
$Fe^{II}-O_2$	0.8780	1.1139
$Fe^{II}-O_3$	1.0195	1.1516

in Raman spectra, while the latter are active in infrared (IR) spectra. Being at the center of symmetry, the Fe atom remains undisplaced in the g-symmetry modes. Only u-symmetry modes are sensitive to the iron isotope. The computed isotope sensitivity is listed in Table 5 as $1 - {}^{56}\nu/{}^{54}\nu$. Also listed is the computed IR intensity, since this will be important to the discussion of IR assignments.

The Fe−O stretching and bending modes are found below 1000 cm^{-1}, as are three kinds of librational modes of the bound H_2O (Figure 2): twisting, wagging, and rocking. The computed frequency order is rocking > wagging > twisting. This seems reasonable, given that rocking occurs in the $FeOH_2$ plane, while wagging is an out-of-plane mode, and twisting involves torsion about the Fe−O bond. It is also the order derived in an early experimental and normal coordinate study by Nakagawa and Shimanouchi,[25] although Adams and Lock,[67] and also Jain,[68] have given arguments for reversing the order of the rocking and wagging modes. Inclusion of the PCM has a significant effect on the computed frequencies. The rocking modes shift up from the ~650 to the ~750 cm^{-1} region, while the wagging modes diminish from ~520 to ~320 cm^{-1}; the twisting modes also diminish somewhat. These shifts reflect the geometric and bonding changes induced by the PCM, as discussed above.

In the T_h structure of $Fe(H_2O)_6^{3+}$, the wagging and rocking modes are degenerate (T_u) as are the g-twisting modes (T_u), but the u-twisting modes have E_u and A_u phasing, with quite different computed frequencies. In the S_6 structure the T_g and T_u degeneracies are lifted, and substantial splittings are computed. For $Fe(H_2O)_6^{2+}$ (C_i structure) all modes are nondegenerate, and large frequency spreads are computed for each mode

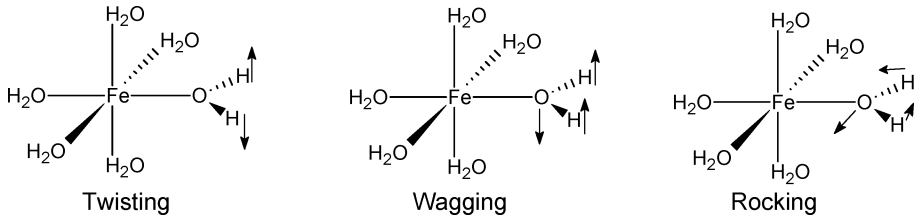

Figure 2. Schematic representation of twisting, wagging, and rocking vibrational coordinates of bound H_2O.

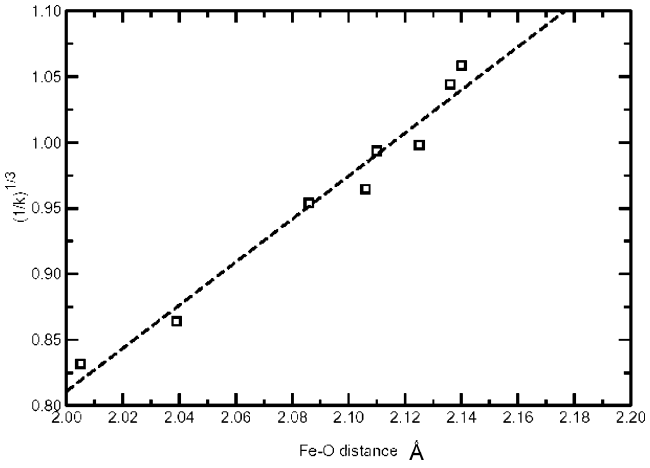

Figure 3. Correlation plot for Badger's rule,[62−64] $R_{eq} = D_{Fe,O} + C_{Fe,O}(1/k)^{1/3}$; best fit values $D_{Fe,O} = -2.462$, $C_{Fe,O} = 1.636$, $R = 0.9838$.

type, especially under the influence of the PCM, which induces large differences among the tilt and rotation coordinates of the water molecules (Table 2).

The Fe−O stretches fall in the 300−500 cm^{-1} region. They shift up significantly when the PCM is applied, reflecting the contraction of the Fe−O bonds (Tables 1 and 2) and the accompanying increase in the force constants (Table 6). They are higher for $Fe(H_2O)_6^{3+}$ than for $Fe(H_2O)_6^{2+}$, as expected. The six Fe−O stretching coordinates of an FeO_6 octahedron are grouped into three modes, of A_{1g}, E_g, and T_{1u} symmetry. The degeneracies are maintained in the T_h ab initio structure of $Fe(H_2O)_6^{3+}$, for which the computed frequencies are 449, 360, and 434 cm^{-1}, respectively. The PCM shifts all of these frequencies up by ∼40 cm^{-1} and splits the T_u mode into A_u and E_u components, with a 17 cm^{-1} splitting (due to the tilting and rotation of the water molecules; the magnitude of the splitting is uncertain because of the doubtful reliability of the PCM-induced water tilting, but it has little consequence for the average Fe−O frequency, which is determined by the bond distance). The three inequivalent Fe−O bonds in $Fe(H_2O)_6^{2+}$ remove all degeneracies, but the octahedral parentage is evident in the near coincidence of modes correlating with A_g and T_{1u} symmetries (∼370 cm^{-1}) and the much lower positions (∼230 cm^{-1}) of the E_g-derived modes.

The O−Fe−O angle bending coordinates of octahedral FeO_6 group into E_g, T_{2g}, T_{1u}, and T_{2u} modes. Again the degeneracies are maintained in the T_h structure of $Fe(H_2O)_6^{3+}$. (However the "1" and "2" labels are lost; consequently the T_{2u} bend, which is spectroscopically inactive in the O_h point group, becomes allowed in the IR spectrum of $Fe(H_2O)_6^{2+}$.) The bending mode positions are all predicted to be between 90 and 200 cm^{-1}, with somewhat higher values for $Fe(H_2O)_6^{3+}$ than for $Fe(H_2O)_6^{2+}$; application of the PCM influences the positions to a small extent.

Although the Fe−O stretches and bends are clearly distinguishable from the water librational modes, there is some mixing of the coordinates. This can be seen in the small but nonnegligible Fe isotope shifts calculated for the water modes (Table 5), especially the wagging and rocking modes. For $Fe(H_2O)_6^{2+}$ the shifts associated with the wagging modes are almost as large as those of the Fe−O stretches, in the in vacuo computation, and about half as large in the PCM model. This mixing has important consequences for the evaluation of equilibrium isotope effects (see below). The effects of the PCM on this mixing are variable and mode-dependent.

Raman and Infrared Spectra. Available mode frequencies from Raman and IR spectra are listed in Tables 4 and 5. The data are from crystalline salts, whose vibrational bands are better resolved than are bands of the complexes in solution, and which are unobscured by contributions from bulk water. The water modes themselves are nevertheless difficult to assign;[69] some correspondences of reported bands with the computed frequencies are noted in the tables, but do not merit further discussion.

The Fe−O stretches and bends, however, are relatively secure. Detailed Raman investigations have been carried out with the aid of oriented single crystals, including the cesium sulfate and selenate alums of $Fe(H_2O)_6^{3+}$,[23] and SiF_6^{2-} and TiF_6^{2-} salts of $Fe(H_2O)_6^{2+}$.[24] Replacement of H_2O with D_2O was used to distinguish Fe−O vibrations from water modes. Infrared spectra have been reported for polycrystalline samples of $Fe(H_2O)_6^{3+}$ alums[70] and of $Fe(H_2O)_6^{2+}$ in the SiF_6^{-2} salt.[25] IR assignments were based on trends among hexaaquo ions and, for $Fe(H_2O)_6^{3+}$, on measured $^{50/53}Cr$ isotope shifts in the isotopic chromium alum.

The assigned Fe−O stretching bands are in reasonable accord with the DFT predictions. For $Fe(H_2O)_6^{2+}$ the agreement is within 10−20 cm^{-1}. However, the discrepancies increase for $Fe(H_2O)_6^{3+}$: the experimental values are 20−75 cm^{-1} higher than the computed values (PCM). (We assign the reported IR bands to the ν_3 component with the highest computed IR intensity.) For the O−Fe−O bending modes, the discrepancies are much larger: observed bands are 100−150 cm^{-1} higher than computed modes for both complexes (though no ν_4 band has been reported for $Fe(H_2O)_6^{2+}$).

What is the source of these large discrepancies? We considered the possibility of basis set dependence of the computed results, or dependence on the level of theory. However, trial calculations with extra diffuse and polarization functions on Fe, O, and H produced only small changes in the mode frequencies, as did switching to a different density functional, B3PW91. As mentioned above, the issue of scaling was considered, but the Fe−O scaling factors given by Pulay and co-workers[38] changed the frequencies very little. We note that Pulay and co-workers obtained accurate mode frequencies for the metal acetylacetonates, including the bending modes, so it seems unlikely that DFT would fail for hexaaquo complexes.

We suggest that the discrepancies are instead attributable to the effects of crystal forces on the mode frequencies, effects which are not included in the calculations. Although application of PCM to the in vacuo calculation introduces polarization effects representative of liquid water, the effects of directional H-bonds are not included. As noted above, these are clearly revealed in the alum neutron structures of $Fe(H_2O)_6^{3+}$, and are

no doubt present in $Fe(H_2O)_6[SiF_6]$ as well. These are expected to alter the potential surface of the complexes, especially with respect to the O−Fe−O bending coordinates. The directional H-bonds anchor the water molecule and raise the effective force constants for O−Fe−O bending. Although H-bonds also form with solvent molecules, they are not rigid anchors, as they are in the crystals. The proposal that lattice forces elevate the bending frequencies is supported by Jenkins and Lewis' finding[24] that the ν_5 doublet of $Fe(H_2O)_6(SiF_6)$, seen at 210/231 cm^{-1} at 15 K, shifted down to 187/198 cm^{-1} at 300 K. At the same time, a shift of low-frequency lattice modes signaled a phase change at low temperature. We suggest that the high-temperature phase allows greater mobility of the bound water molecules, as signaled by diminished O−Fe−O bending frequencies.

Although the bending modes are most sensitive to the presence of directional H-bonds, it is plausible that the Fe−O stretching modes are also somewhat affected, and that the smaller, but still sizable discrepancies between observed and computed frequencies of these modes can be similarly understood. Indeed, 20−30 cm^{-1} differences have been noted between solution and crystalline phases of several aquo ions.[69] Specifically, a totally symmetric Fe−O stretch ν_1 has been observed in aqueous solution for ferric complex and ferrous complex[71] at 506 and 380 cm^{-1}, respectively, which substantially reduce the discrepancies between the observed and the PCM-predicted ν_1 modes.

Iron Isotope Fractionation Equilibrium. The possibility of calculating equilibrium constants for isotopic exchange reactions from spectroscopic data alone was first pointed out by Urey and Rittenberg.[72] Equilibrium isotope fractionations arise from the sensitivity of vibrational frequencies to atomic masses. The influence of vibrations on the isotopic exchange equilibrium constant, α^{kl}, between two compounds, *k* and *l*, is expressed in terms of the vibrational partition functions for two isotopomers *a* and *b*: $\ln[\alpha^{kl}] = {}^{a-b}\beta_k - {}^{a-b}\beta_l$, where ${}^{a-b}\beta = \ln[{}^aQ_{vib}/{}^bQ_{vib}]$ and $Q_{vib} = \prod_i \exp(-h\nu_i/2kT)/(1 - \exp(-h\nu_i/kT))$. The usual practice, which we follow here, is to report reduced partition function ratios β, by subtracting a constant, $\ln[\prod_i({}^b\nu_i/{}^a\nu_i)] = \ln[(m_a/m_b)^{3/2}(M_b/M_a)^{3/2}]$ from the $\ln({}^aQ_{vib}/{}^bQ_{vib})$ value, which brings the β value to zero in the high-temperature limit. For $a = {}^{56}Fe$ and $b = {}^{54}Fe$, where *m* and *M* are the masses of Fe and of $Fe(H_2O)_6$, this constant is 36.124×10^{-3}.

Schauble et al.[27] applied these equations to the computation of ${}^{56}Fe/{}^{54}Fe$ isotope fractionation between the Fe^{3+} and Fe^{2+} hexaaquo complexes. To obtain isotope shifts, they fit an empirical force field (modified Urey−Bradley, MUBFF) to the vibrations of an MO_6 octahedron, using reported stretching (ν_3) and bending (ν_4) frequencies (Table 5): 505 and 304 cm^{-1} for Fe^{3+} and 389 and 195 cm^{-1} for Fe^{2+} (the last value was not actually observed, but came from an earlier MUBFF calculation by Nakagawa and Shimanouchi[25]). The resulting reduced partition function ratios (at 22 °C) were ${}^{56-54}\beta = 11.78 \times 10^{-3}$ and 6.35×10^{-3} for Fe^{3+} and Fe^{2+}, giving an equilibrium of isotope fractionation factor $\alpha = 1.0054$.

In contrast, the present DFT-derived isotopic shifts give ${}^{56-54}\beta = 9.30 \times 10^{-3}$ and 6.82×10^{-3} for Fe^{3+} and Fe^{2+}, and $\alpha = 1.0025$. (This is for the PCM model; the in vacuo numbers differ only slightly, ${}^{56-54}\beta = 9.63 \times 10^{-3}$ and 6.68×10^{-3}, and $\alpha = 1.0030$. Thus the structural distortions of the PCM model are unimportant in this context.) How does the difference with respect to Schauble et al. arise? There are two sources: (1) the frequencies differ for the two calculations, and (2) the computation of all the $M(H_2O)_6$ modes in the DFT model spreads the isotope shifts into water librational modes, as well as the M−O stretches and bends. The product of all the isotope frequency ratios is the same for the two computations, as they must be (Redlich−Teller rule).

The frequency differences account for most of the discrepancy. This can be demonstrated by retaining the MUBFF isotope frequency ratios (${}^{56}\nu/{}^{54}\nu = 0.9943$ and 0.9937 for ν_3 and ν_4 of Fe^{3+}, and 0.9937 and 0.9943 for ν_3 and ν_4 of Fe^{2+}) and changing the frequencies to those computed by DFT (averages of the three T_{2u} components; see Table 5): 475 and 180 cm^{-1} for ν_3 and ν_4 of Fe^{3+}, and 379 and 142 cm^{-1} for ν_3 and ν_4 of Fe^{2+}. The result is $\alpha = 1.0031$. Thus 80% of the difference with respect to the DFT PCM treatment ($\alpha = 1.0025$) is due to the difference in frequencies, while the remainder is attributable to the spreading out of the isotope shifts. Most of the difference is actually attributable to the discrepant bending frequency, ν_4, of Fe^{3+}. As discussed above the DFT-computed frequency is much lower than the observed band in the alum spectrum, an effect attributable to rigid H-bonds in the crystal. If all MUBFF frequencies are retained except for ν_4 of Fe^{3+}, then $\alpha = 1.0036$. Thus the lowering of this one frequency moves the fractionation factor 2/3 of the way to the DFT PCM value.

Both DFT PCM and in vacuo values are close to the experimental value determined by Johnson et al.[7] and recently refined by Welch et al.,[26] $\alpha = 1.0028-1.0030$ at 22 °C. The present analysis throws light on the large disagreement between the experimental α and the one previously computed from the available vibrational data. The main source of this disagreement can be traced to the use of vibrational spectra on H-bonded crystals, which gives higher Fe−O skeletal frequencies than are computed ab initio, especially for bending frequencies and especially for $Fe(H_2O)_6^{3+}$.

Acknowledgment. The authors thank Pat Holland for suggesting this joint effort, the Gordon Research Conferences for providing an atmosphere conducive to collaboration, and François Morel for early encouragement. Funding was provided by the Center for Environmental Bioinorganic Chemistry (NSF CHE 0221978), and by grants from the NASA Astrobiology Institute and NSF (EAR 0003565) to A.D.A.

References and Notes

(1) Hoefs, J. *Stable Isotope Geochemistry*; Springer-Verlag: New York, 1997.

(2) Anbar, A. D.; Roe, J. E.; Barling, J.; Nealson, K. H. *Science* **2000**, *288*, 126.

(3) Barling, J.; Arnold, G. L.; Anbar, A. D. *Earth Planet. Sci. Lett.* **2001**, *193*, 447.

(4) Beard, B. L.; Johnson, C. M.; Cox, L.; Sun, H.; Nealson, K. H.; Aguilar, C. *Science* **1999**, *285*, 1889.

(5) Bullen, T. D.; White, A. F.; Childs, C. W.; Vivit, D. V.; Schulz, M. S. *Geology* **2001**, *29*, 699.

(6) Ellis, A. S.; Johnson, T. M.; Bullen, T. D. *Science* **2002**, *295*, 2060.

(7) Johnson, C. M.; Skulan, J. L.; Beard, B. L.; Sun, H.; Nealson, K. H.; Braterman, P. S. *Earth Planet. Sci. Lett.* **2002**, *195*, 141.

(8) Marechal, C. N.; Telouk, P.; Albarede, F. *Chem. Geol.* **1999**, *156*, 251.

(9) Rehkamper, M.; Frank, M.; Hein, J. R.; Porcelli, D.; Halliday, A.; Ingri, J.; Liebetrau, V. *Earth Planet. Sci. Lett.* **2002**, *197*, 65.

(10) Siebert, C.; Nägler, T. F.; von Blanckenburg, F.; Kramers, J. D. *Earth Planet. Sci. Lett.* **2003**, *211*, 159.

(11) Wombacher, F.; Rehkamper, M.; Mezger, K.; Munker, C.; Bischoff, A. *Geochim. Cosmochim. Acta* **2002**, *66*, A844.

(12) Zhu, X.-K.; O'Nions, K.; Guo, Y.; Reynolds, B. C. *Science* **2000**, *287*, 2000.

(13) Zhu, X.-K.; Makishima, A.; Guo, Y.; Belshaw, N. S.; O'Nions, R. K. *Int. J. Mass Spectrom.* **2002**, *220*, 21.

(14) Zhu, X.-K.; Guo, Y.; O'Nions, R. K.; Young, E. D.; Ash, R. D. *Nature* **2001**, *412*, 311.
(15) Walczyk, T.; von Blanckenburg, F. *Science* **2002**, *295*, 2065.
(16) Johnson, C. M.; Beard, B. L.; Beukes, N. J.; Klein, C.; O'Leary, J. M. *Contrib. Mineral. Petrol.* **2003**, *144*, 523.
(17) O'Neil, J. R. Theoretical and experimental aspects of isotopic fractionation. In *Stable Isotopes in High Temperature Geological Processes*; Valley, J. W., Taylor, H. P., O'Neil, J. R., Eds.; Mineralogical Society of America: Washington, D.C.,1986; Vol. 16; p 1.
(18) Criss, R. E. *Principles of Stable Isotope Distribution*; University Press: New York, 1999.
(19) Bigeleisen, J.; Mayer, M. G. *J. Chem. Phys.* **1947**, *15*, 261.
(20) Urey, H. *J. Chem. Soc.* **1947**, 562.
(21) Best, S. P.; Forsyth, J. B. *J. Chem. Soc., Dalton Trans.* **1990**, 395.
(22) Cotton, F. A.; Daniels, L. M.; Murillo, C. A.; Quesada, J. F. *Inorg. Chem.* **1993**, *32*, 4861.
(23) Best, S. P.; Beattie, J. K.; Armstrong, R. S. *J. Chem. Soc., Dalton Trans.* **1984**, 2611.
(24) Jenkins, T. E.; Lewis, J. *Spectrochim. Acta, Part A: Mol. Biomol. Spectrosc.* **1981**, *37*, 47.
(25) Nakagawa, I.; Shimanouchi, T. *Spectrochim. Acta* **1964**, *20*, 429.
(26) Welch, S. A.; Beard, B. L.; Johnson, C. M.; Braterman, P. S. *Geochim. Cosmochim. Acta* **2003**, *67*, 4231.
(27) Schauble, E. A.; Rossman, G. R.; Taylor, H. P. *Geochim. Cosmochim. Acta* **2001**, *65*, 2487.
(28) Anbar, A. D.; Jarzecki, A. A.; Spiro, T. G. In revision in *Earth Planet. Sci. Lett.*
(29) Frisch, M. J.; Trucks, G. W.; Schlegel, H. B.; Scuseria, G. E.; Robb, M. A.; Cheeseman, J. R.; Zakrzewski, V. G.; Montgomery, J. A., Jr.; Stratmann, R. E.; Burant, J. C.; Dapprich, S.; Millam, J. M.; Daniels, A. D.; Kudin, K. N.; Strain, M. C.; Farkas, O.; Tomasi, J.; Barone, V.; Cossi, M.; Cammi, R.; Mennucci, B.; Pomelli, C.; Adamo, C.; Clifford, S.; Ochterski, J.; Petersson, G. A.; Ayala, P. Y.; Cui, Q.; Morokuma, K.; Malick, D. K.; Rabuck, A. D.; Raghavachari, K.; Foresman, J. B.; Cioslowski, J.; Ortiz, J. V.; Baboul, A. G.; Stefanov, B. B.; Liu, G.; Liashenko, A.; Piskorz, P.; Komaromi, I.; Gomperts, R.; Martin, R. L.; Fox, D. J.; Keith, T.; Al-Laham, M. A.; Peng, C. Y.; Nanayakkara, A.; Gonzalez, C.; Challacombe, M.; Gill, P. M. W.; Johnson, B. G.; Chen, W.; Wong, M. W.; Andres, J. L.; Head-Gordon, M.; Replogle, E. S.; Pople, J. A. *Gaussian 98*, Revision A.7; Gaussian, Inc: Pittsburgh, PA, 1998.
(30) Becke, A. D. *J. Chem. Phys.* **1993**, *98*, 1372.
(31) Lee, C. T.; Yang, W. T.; Parr, R. G. *Phys. Rev. B* **1988**, *37*, 785.
(32) Harihara, Pc.; Pople, J. A. *Mol. Phys.* **1974**, *27*, 209.
(33) Ditchfie, R.; Hehre, W. J.; Pople, J. A. *J. Chem. Phys.* **1971**, *54*, 724.
(34) Francl, M. M.; Pietro, W. J.; Hehre, W. J.; Binkley, J. S.; Gordon, M. S.; Defrees, D. J.; Pople, J. A. *J. Chem. Phys.* **1982**, *77*, 3654.
(35) Harihara, Pc.; Pople, J. A. *Theor. Chim. Acta* **1973**, *28*, 213.
(36) Hehre, W. J.; Ditchfie, R.; Pople, J. A. *J. Chem. Phys.* **1972**, *56*, 2257.
(37) Schafer, A.; Horn, H.; Ahlrichs, R. *J. Chem. Phys.* **1992**, *97*, 2571.
(38) Diaz-Acosta, I.; Baker, J.; Cordes, W.; Pulay, P. *J. Phys. Chem. A* **2001**, *105*, 238.
(39) Diaz-Acosta, I.; Baker, J.; Hinton, J. F.; Pulay, P. *Spectrochim. Acta, Part A: Mol. Biomol. Spectrosc.* **2003**, *59*, 363.
(40) Jarzecki, A. A.; Kozlowski, P. M.; Pulay, P.; Ye, B. H.; Li, X. Y. *Spectrochim. Acta, Part A: Mol. Biomol. Spectrosc.* **1997**, *53*, 1195.
(41) Kozlowski, P. M.; Rush, T. S.; Jarzecki, A. A.; Zgierski, M. Z.; Chase, B.; Piffat, C.; Ye, B. H.; Li, X. Y.; Pulay, P.; Spiro, T. G. *J. Phys. Chem. A* **1999**, *103*, 1357.
(42) Tomasi, J.; Persico, M. *Chem. Rev.* **1994**, *94*, 2027.
(43) Cossi, M.; Barone, V.; Cammi, R.; Tomasi, J. *Chem. Phys. Lett.* **1996**, *255*, 327.
(44) Coitino, E. L.; Tomasi, J.; Cammi, R. *J. Comput. Chem.* **1995**, *16*, 20.
(45) Cances, E.; Mennucci, B.; Tomasi, J. *J. Chem. Phys.* **1997**, *107*, 3032.
(46) Amovilli, C.; Barone, V.; Cammi, R.; Cances, E.; Cossi, M.; Mennucci, B.; Pomelli, C. S.; Tomasi, J. Recent advances in the description of solvent effects with the polarizable continuum model. *Adv. Quantum Chem.* **1999**,*32*, 227.
(47) Rudolph, W. W.; Mason, R.; Pye, C. C. *Phys. Chem. Chem. Phys.* **2000**, *2*, 5030.
(48) Rudolph, W. W.; Pye, C. C. *J. Solution Chem.* **2000**, *29*, 955.
(49) Magini, M. *J. Inorg. Nucl. Chem.* **1978**, *40*, 43.
(50) Armstrong, R. S.; Beattie, J. K.; Best, S. P.; Skelton, B. W.; White, A. H. *J. Chem. Soc., Dalton Trans.* **1983**, 1973.
(51) Armstrong, R. S.; Beattie, J. K.; Best, S. P.; Braithwaite, G. P.; Delfavero, P.; Skelton, B. W.; White, A. H. *Aust. J. Chem.* **1990**, *43*, 393.
(52) Best, S. P.; Forsyth, J. B. *J. Chem. Soc., Dalton Trans.* **1991**, 1721.
(53) Tregenna-Piggott, P. L. W.; Best, S. P.; O'Brien, M. C. M.; Knight, K. S.; Forsyth, J. B.; Pilbrow, J. R. *J. Am. Chem. Soc.* **1997**, *119*, 3324.
(54) Tregenna-Piggott, P. L. W.; Andres, H. P.; McIntyre, G. J.; Best, S. P.; Wilson, C. C.; Cowan, J. A. *Inorg. Chem.* **2003**, *42*, 1350.
(55) Beattie, J. K.; Best, S. P.; DelFavero, P.; Skelton, B. W.; Sobolev, A. N.; White, A. H. *J. Chem. Soc., Dalton Trans.* **1996**, 1481.
(56) Tregenna-Piggott, P. L. W.; Best, S. P. *Inorg. Chem.* **1996**, *35*, 5730.
(57) Tregenna-Piggott, P. L. W.; Best, S. P.; Gudel, H. U.; Weihe, H.; Wilson, C. C. *J. Solid State Chem.* **1999**, *145*, 460.
(58) Dolder, S.; Spichiger, D.; Tregenna-Piggott, P. L. W. *Inorg. Chem.* **2003**, *42*, 1343.
(59) Armstrong, R. S.; Berry, A. J.; Cole, B. D.; Nugent, K. W. *J. Chem. Soc., Dalton Trans.* **1997**, 363.
(60) Dubicki, L.; Bramley, R. *Chem. Phys. Lett.* **1997**, *272*, 55.
(61) Kallies, B.; Meier, R. *Inorg. Chem.* **2001**, *40*, 3101.
(62) Badger, R. *J. Chem. Phys.* **1934**, *2*, 128.
(63) Badger, R. *J. Chem. Phys.* **1934**, *3*, 131.
(64) Badger, R. *J. Chem. Phys.* **1935**, *3*, 710.
(65) Rauhut, G.; Pulay, P. *J. Am. Chem. Soc.* **1995**, *117*, 4167.
(66) Baker, J.; Jarzecki, A. A.; Pulay, P. *J. Phys. Chem. A* **1998**, *102*, 1412.
(67) Adams, D. M.; Lock, P. J. *J. Chem. Soc. A: Inorg. Phys. Theor.* **1971**, 2801.
(68) Jain, Y. S. *Solid State Commun.* **1975**, *17*, 605.
(69) Best, S. P.; Armstrong, R. S.; Beattie, J. K. *J. Chem. Soc., Dalton Trans.* **1992**, 299.
(70) Best, S. P.; Armstrong, R. S.; Beattie, J. K. *Inorg. Chem.* **1980**, *19*, 1958.
(71) Kanno, H. *J. Phys. Chem.* **1988**, *92*, 4232.
(72) Urey, H.; Rittenberg, D. *J. Chem. Phys.* **1933**, *1*, 137.
(73) Reed, A. E.; Curtiss, L. A.; Weinhold, F. *Chem. Rev.* **1988**, *88*, 899.